Evolution of wall shear stress with Reynolds number in fully developed turbulent channel flow experiments

Pierre-Alain Gubian, Jordan Stoker, James Medvescek, Laurent Mydlarski,[*] and B. Rabi Baliga
Department of Mechanical Engineering, McGill University, Montreal, QC, H3A 0C3, Canada

(Received 21 October 2018; published 26 July 2019)

The Reynolds-number-dependence of wall shear stress (τ_w) in fully developed, high-aspect-ratio turbulent channel flow is experimentally studied over the range of $230 \leqslant \mathrm{Re}_\tau \leqslant 950$. The principal conclusion of the present work is that beyond $\mathrm{Re}_\tau \sim 600$, the wall shear stress evolves to an asymptotic state in which the statistical moments, probability density function, and power spectra of τ_w become independent of Reynolds number. In this state, the turbulent intensity, skewness and kurtosis of the wall shear stress take on values that are slightly larger than those previously measured, because prior estimates of these quantities did not resolve the full range of wall shear stress fluctuations, which extended beyond 10 standard deviations above the mean. For $\mathrm{Re}_\tau \gtrsim 600$, the spectra of τ_w were found to collapse very well when using a wall-unit-based normalization, providing further evidence of an asymptotic state of the wall shear stress at large Reynolds numbers.

DOI: 10.1103/PhysRevFluids.4.074606

I. INTRODUCTION

Since the publication of Kolmogorov's [1] seminal theory on the (possibly universal) scaling of turbulent flows, there have been many investigations of the small-scale structure of turbulence. (See Sreenivasan and Antonia [2] for an overview.) However, it bears noting that Kolomogorov theory is only valid in the limit of infinite Reynolds number and that finite-Reynolds-number effects may be present and significant in many flows. Moreover, many, if not most, industrial flows occur at moderate Reynolds numbers, which cannot be deemed "infinitely large" (in the Kolmogorovian sense). These observations have motivated the study of finite-Reynolds-number effects in turbulent flows, although this topic has only been a significant focus of research more recently [3–20]. For the most part, the study of finite-Reynolds-number effects in turbulent flows has focused on the velocity field, although some exceptions do exist (e.g., Refs. [18,21–24]). The purpose of the research reported in this paper is to experimentally investigate the Reynolds number dependence of the wall shear stress in fully developed turbulent channel flow, to complement the existing body of work on finite-Reynolds-number effects on the velocity field. In the present work, a high-aspect-ratio duct is used to model a channel flow. The primary objective of this investigation is to determine whether the wall shear stress achieves an asymptotic state in the limit of sufficiently large Reynolds numbers and, if so, to quantify it. This objective is pursued by way of highly resolved experimental measurements of the instantaneous wall shear stress over a range of Reynolds numbers surpassing that of prior experimental investigations on this subject.

Unlike investigations of the wall shear stress in external turbulent flows (e.g., turbulent boundary layers), of relevance to fields such as aerodynamics, the present work focusses on internal flows, which are also encountered in many practical applications (e.g., the transport for fluids in pipes and pipelines; and heating, ventilation and air conditioning systems). The object of the present

[*]Corresponding author: laurent.mydlarski@mcgill.ca

investigation is a fully developed turbulent channel flow, because it is the simplest expression of an inhomogeneous turbulent flow, being statistically inhomogeneous in only one (the wall-normal) direction, and homogeneous in the other two (downstream and spanwise) directions. We therefore proceed to provide a brief review of prior investigations of wall shear stress in fully developed turbulent (duct and) channel flows.

Mitchell and Hanratty [25], Popovich [26], Eckelmann [27], Sreenivasan and Antonia [28], and Chambers *et al.* [29] were among the pioneers in making instantaneous measurements of the wall shear stress in duct and channel flows. However, as noted by Alfredsson *et al.* [30], early measurements of wall shear stress suffered from limitations in the sensors that were related to issues of frequency response, spatial resolution and/or heat loss to the wall (in the case of sensors based on thermal anemometry), which results in underestimates of the wall shear stress fluctuations. (For further analysis on the issue of spatial resolution of shear stress estimates in wall-bounded flows, see Örlü and Schlatter [31]). In their work, Alfredsson *et al.* [30] measured the fluctuating wall shear stress in boundary layer and channel flows using different fluids (air, oil, and water) at bulk Reynolds numbers of 3800, 5000, and 28 000 (where the respective characteristic lengths were the boundary-layer thickness or the channel half-height, and the characteristic velocities were the free-stream or centreline velocities). Alfredsson *et al.* [30] concluded that the turbulent intensity of the fluctuating wall shear stress was 40%, and its skewness and kurtosis were close to 1.0 and 4.8, respectively. Obi *et al.* [32] used an optical (laser-based) approach to study the wall shear stress in turbulent channel flow in which air was the working fluid for bulk Reynolds numbers of 5600 and 6600. Consistent with the results of Alfredsson *et al.* [30], they found the turbulence intensity, skewness, and kurtosis of the wall shear stress fluctuations to be around 35–41%, 0.95–1.05, and 4.6–4.7, respectively. However, the observed variations of these quantities with the Reynolds number were less then the experimental uncertainty. Using a micro-electromechanical-system (MEMS)-based micro-shear-stress imaging chip, Miyagi *et al.* [33] measured the fluctuating wall shear stress in a channel flow for bulk Reynolds numbers ranging from 8758 to 17 517. They concluded that the probability density functions (PDFs) of the fluctuating wall shear stress all overlapped when the fluctuations were normalized by their root-mean-square values, and that the turbulence intensity, skewness, and kurtosis of the wall shear stress fluctuations were approximately 40%, 1.09, and 4.6, respectively. Using flush-mounted hot-wire sensors operated by a constant-temperature anemometer, Khoo *et al.* [34] measured the wall shear stress in both turbulent channel and boundary layers flows, for which the former had friction Reynolds numbers ($\mathrm{Re}_\tau = u_\tau h/\nu$) of 180 and 390, where $u_\tau(\equiv\sqrt{\tau_w/\rho})$ is the friction velocity, ρ is the density of the fluid, h is the channel half-height, and ν is the kinematic viscosity of the fluid. They measured PDFs and spectra of τ_w and observed a reasonable collapse of the latter when nondimensionalized using wall units. Using a micro-pillar-based sensor, Große and Schröder [35,36] and Gnanamanickam *et al.* [37] undertook wall shear stress measurements in turbulent pipe and duct flows, for bulk Reynolds numbers (based on the mean bulk velocity and duct diameter/height) in the range of 10 000 to 20 000. They measured statistical moments of τ_w up to fourth order, but their measurement approach suffered from limitations of the sensor pertaining to its sensitivity in gaseous flows, frequency response/resonance, and reduced resolution at higher Reynolds numbers. Nevertheless, their measurement approach holds high promise for measuring the two-dimensional, unsteady wall shear stress distribution. Using an electrochemical method, Keirsbulck *et al.* [38] measured the wall shear stress in turbulent channel flow over the range $74 \leqslant \mathrm{Re}_\tau \leqslant 400$. Their results were consistent with previous measurements of the turbulent intensity, skewness, and kurtosis of τ_w. Moreover, they found the wall shear stress spectra to also collapse using wall-unit scaling over their range of Reynolds numbers. However, they did not observe any asymptotic regime over the range of Reynolds numbers studied. Amili *et al.* [39] investigated the wall shear stress in turbulent channel flow by way of a novel sensor that used the deformation of a thin elastic film as its working principle. They, however, only made measurements of ensemble- and spatially-averaged wall shear stress.

With respect to direct numerical simulations (DNSs) of fully developed turbulent channel flow, seminal work was undertaken by Kim *et al.* [40] and Moser *et al.* [41], the latter finding turbulent intensities of τ_w from 0.363 to 0.405, for Re_τ varying from 180–590. Abe *et al.* [23] also investigated the evolution with Reynolds number of fully developed turbulent flows in a channel, for values of $\mathrm{Re}_\tau = 180,\ 395$, and 640, by way of direct numerical simulations and found the turbulent intensity of τ_w to be 0.409 at their highest Reynolds number. Of particular interest is the work of Hu *et al.* [24] and Lenaers *et al.* [42], who undertook simulations that are the most similar to the experiments undertaken herein, given that they were (i) undertaken at Reynolds numbers that equal (and exceed) those herein and (ii) focused on the wall shear stress. The work of Lee and Moser [43] is also relevant, as their channel flow simulations extended over the range $180 \leqslant \mathrm{Re}_\tau \leqslant 5186$. Although their simulations did not explicitly focus on the wall shear stress, data on wall shear stress was extracted from their results.

Having provided an introduction and a brief review of the literature, the remainder of this paper is organized as follows. The apparatus and instrumentation are described in Sec. II. The results are presented and discussed in Sec. III. Finally, concluding remarks are given in Sec. IV.

II. APPARATUS AND INSTRUMENTATION

The present experiments were undertaken in an open-circuit, high-aspect-ratio channel facility in the Aerodynamics Laboratory of the Department of Mechanical Engineering at McGill University, which has a 8.0 m $\times$ 1.1 m $\times$ 0.060 m ($L \times H \times W$) test section. As noted in the previous section, the high-aspect-ratio duct is used in the present work to model a channel flow. The magnitude of the duct aspect ratio required to accurately model a channel flow has been investigated by Vinuesa *et al.* [44–46], who initially recommended aspect ratios of at least 24 to minimize the effects of sidewalls in turbulent duct experiments. However, in their later work, further analysis led them to relax their requirement and they "conclude that since long-time averages of statistics in the core region of rectangular ducts, spanning about the width of a well-designed channel simulation (i.e., extending about $\simeq 3h$ on each side of the center plane), are similar to results from computations of the canonical channel flow, one may utilize ducts or experimental facilities with aspect ratios larger than 10 to compare their time-averaged information with results obtained from spanwise-periodic channel simulations" [46]. The half-width ($h = W/2$) of the test section of the channel used herein is 0.030 m, and its aspect ratio ($H/W = H/2h$) is 18.3. Moreover, measurements undertaken in the same facility at three different spanwise positions by Lepore and Mydlarski [47] (see Fig. 3 therein) have confirmed that the flow at the channel midspan is statistically two-dimensional. At the entrance to the test section, the boundary layers on both walls ($y = 0$ and $y = 2h$) are tripped to accelerate the development of the flow to its fully developed state. (x, y, and z are the streamwise, wall-normal, and spanwise directions, respectively). Two 3.2-mm-diameter rods were installed 3 mm from each wall to trip the boundary layers. The rods were located 60 mm downstream of the entrance to the test section, to allow for some boundary-layer growth before tripping them. Measurements undertaken in the same facility at different downstream positions by Lavertu and Mydlarski [48] (see Fig. 3 therein) confirmed the fully developed nature of the flow at the measurement location. Consequently, the flow under consideration is a statistically one-dimensional flow (i.e., $\langle U \rangle = \langle U(y) \rangle$ only). The channel and the velocity field therein have been extensively described in Refs. [47–50], thus the discussion herein of the apparatus and the flow will be relatively succinct.

Two types of thermal-anemometry-based measurements were performed. First, hot-wire anemometry was used to measure the instantaneous longitudinal velocity at the channel centreline, to establish the flow conditions. To this end, a TSI 1210 probe with a 3.05-μm-diameter tungsten wire was operated with an overheat of 1.8, using a TSI IFA 300 constant-temperature hot-wire anemometer [47–52]. The length-to-diameter ratio of the sensing portion of the sensor wire was approximately 200, and the hot-wire probe was calibrated using a TSI 1128 calibration jet. Second, wall-shear-stress measurements were made using a novel, high-spatial and high-temporal-resolution, thermal-anemometry-based wall-shear-stress sensor, inspired by the designs of Spazzini *et al.* [53] and Sturzebecher *et al.* [54]. It consists of a custom-made, flush-mounted, hot-wire sensor, in which the hot-wire is installed over a small rectangular cavity in the sensor's base and

TABLE I. Flow parameters. Recall $h = 0.03$ m is the channel half-width (and the channel mid-plane is at $y/h = 1$). $\tau'_w = \tau_w - \langle\tau_w\rangle$. $x/h = 222$, $D_h[=4A_{cs}/P = 4HW/(2H+2W)] = 0.114$ m, $\nu = 15 \times 10^{-6}$ m^2 s^{-1}, $\rho = 1.2$ kg m^{-3}. T is the sampling period.

$\langle U(y/h=1)\rangle$ (m s^{-1})	1.99	3.52	4.85	5.30	6.14	7.59	8.97	10.4	11.1
$u_{\mathrm{RMS}}(y/h=1)$ (m s^{-1})	0.0849	0.137	0.193	0.203	0.236	0.281	0.338	0.390	0.415
$\langle\tau_w\rangle$ (Pa)	0.0162	0.0338	0.0604	0.0709	0.0954	0.137	0.186	0.240	0.273
$u_\tau(=\sqrt{\langle\tau_w\rangle/\rho}\,)$ (m s^{-1})	0.116	0.168	0.224	0.243	0.282	0.338	0.394	0.448	0.477
$\tau_{w_{\mathrm{RMS}}}(=\sqrt{\langle(\tau'_w)^2\rangle})$ (Pa)	0.00454	0.0126	0.0251	0.0302	0.0417	0.0611	0.0832	0.107	0.121
$\tau_{w_{\mathrm{RMS}}}/\langle\tau_w\rangle$	0.281	0.374	0.415	0.427	0.437	0.444	0.447	0.446	0.444
$S_{\tau_w}(=\langle{\tau'_w}^3\rangle/\langle{\tau'_w}^2\rangle^{3/2})$	1.13	1.31	1.35	1.37	1.41	1.41	1.44	1.43	1.40
$K_{\tau_w}(=\langle{\tau'_w}^4\rangle/\langle{\tau'_w}^2\rangle^2)$	4.93	5.89	6.24	6.27	6.60	6.58	6.70	6.65	6.38
$\mathrm{Re}_\tau(=u_\tau h/\nu)$	232	336	449	486	564	677	788	895	954
$\mathrm{Re}_{D_h}(=\langle U(y/h=1)\rangle D_h/\nu)$	15 100	26 700	36 800	40 200	46 600	57 600	68 000	78 700	84 300
$D^+_{\mathrm{sensor}}(=D_{\mathrm{wire}}u_\tau/\nu)$	0.0193	0.0280	0.0374	0.0405	0.0470	0.0564	0.0657	0.0746	0.0795
$L^+_{\mathrm{sensor}}(=L_{\mathrm{wire}}u_\tau/\nu)$	9.67	13.0	18.7	20.2	23.5	28.2	32.8	37.3	39.8
$A^+_{\mathrm{sensor}}(=D^+_{\mathrm{sensor}}L^+_{\mathrm{sensor}})$	0.187	0.391	0.699	0.820	1.10	1.59	2.16	2.78	3.16
f_{sampling} (kHz)	0.4	1.6	2.8	3.4	6.5	9.0	11.2	15.2	16.8
T (s)	205	307	293	304	300	300	293	216	195
$u_\tau T/h$	793	1719	2188	2462	2820	3380	3848	3226	3101

is flush with the channel wall. The purpose of the small (1-mm-wide by 0.1-mm-deep) cavity is to avoid direct contact and minimize conduction from the hot wire to the sensor's substrate, which greatly increases the sensor's frequency response (>10 kHz). The hot wire (i) consisted of a 2.5-μm-diameter tungsten wire operated with an overheat of 1.5, using a DISA 55M10 constant-temperature hot-wire anemometer, and (ii) had a length-to-diameter ratio of 500. The sensor was calibrated in a rectangular mini-channel in the Heat Transfer Laboratory of the Department of Mechanical Engineering at McGill University, which was designed for this purpose. During both the calibration and experiments, particular care was taken to ensure that the sensor was flush with the channel walls. To this end, special jigs were designed to keep the offset between the sensor and channel wall to within $\pm\ 2.5 \times 10^{-5}$ m. The details of the design, construction, calibration, operation, and validation of the wall-shear-stress sensor are given in Ref. [55].

The output voltages of both anemometers were high- and low-pass filtered, sampled at 2–2.5 times the Kolmorogov frequency, and digitized with a National Instruments 16-bit data acquisition card (NI PCI 6221). The sampling frequency (f_{sampling}) depended on the Reynolds number of the flow, varied from 400 Hz to 16.8 kHz, and is listed in Table I for each experiment. The data was acquired using a computer program written in LabVIEW, and subsequently analyzed to calculate statistical moments, probability density functions (PDFs), power spectral densities, etc. The sampling period for each experiment varied from 195 s to 307 s, and the nondimensionalized sampling period ($u_\tau T/h$, i.e., the number of turnover times for eddies of scale h and velocity u_τ within the sampling period T; Lenaers *et al.* [42]) varied from 793 to 3848. Thus, the data record lengths of the experiments varied from 8.192×10^4 samples at the lowest Reynolds number to 3.277×10^6 samples at the largest one. The statistical convergence of the data presented in Sec. III was confirmed (for statistics up to fourth order) by convergence tests, which demonstrated that the fourth-order statistics were converged within the first 20% of the record, and lower-order statistics converged even more rapidly. The parameters of the cases studied herein are given in Table I.

Using the procedures outlined in AMSE-PTC-19.1-2005 [56], the uncertainty in the estimates of the wall-shear stress is found to be ±2.5%, noting that the uncertainty in the height of the calibration mini-channel and the mass flow rate of air within it dominated all other sources of error (angular offset of the sensor, resolution of the data acquisition card, calibration curve-fit, offset of the sensor from being flush mounted, and temperature effects). Furthermore, assuming that the uncertainty of

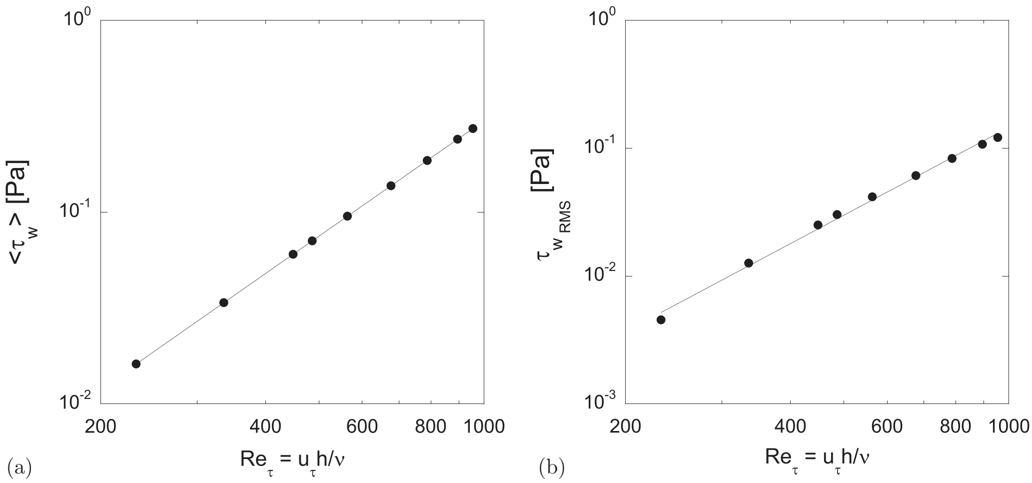

FIG. 1. The dependence of the (a) average and (b) RMS wall shear stress on friction Reynolds number ($\mathrm{Re}_\tau \equiv u_\tau h/\nu$, where h is the channel half-width).

the estimates of the density, viscosity, and channel half-width are negligible compared to those of the wall shear stress, the uncertainty in the quoted friction Reynolds numbers will be at most $\pm 1.3\%$, since the friction velocity is proportional to the square root of the mean wall shear stress. It is worth noting that uncertainties may also be quantified using alternate approaches, e.g., Refs. [57,58].

III. RESULTS AND DISCUSSION

In this section, we present results pertaining to the statistics of the wall shear stress (τ_w) measured in fully developed turbulent flows in a high-aspect-ratio channel (described in the previous section). In particular, we emphasize the Reynolds number dependence of these statistics, which are evaluated over the range $230 \leqslant \mathrm{Re}_\tau \leqslant 950$.

We begin by plotting the mean and root-mean-square of the fluctuations of the wall shear stress about the mean (denoted as $\langle \tau_w \rangle$ and $\tau_{w_{\mathrm{RMS}}}$, respectively) as a function of Reynolds number in Figs. 1(a) and 1(b), respectively. As might be expected, we observe a monotonic increase in $\langle \tau_w \rangle$ with increasing Re_τ. Moreover, it is worth noting that the increase is not linear; it is exactly quadratic [as testified by a best-fit power-law to the data of Fig. 1(a)]. This is a direct result of the relationship between τ_w and $u_\tau \equiv (\tau_w/\rho)^{1/2}$. The dependence of $\tau_{w_{\mathrm{RMS}}}$ on Re_τ appears to be qualitatively very similar—monotonically increasing with increasing Re_τ. However, when examined quantitatively, $\tau_{w_{\mathrm{RMS}}}$ is found to increase at a more rapid rate than $\langle \tau_w \rangle$. Specifically, a least-squares power-law fit to the data demonstrates that $\tau_{w_{\mathrm{RMS}}} \propto \mathrm{Re}_\tau^{2.28}$, although the quality of the fit is best at lower Reynolds numbers, and the $\tau_{w_{\mathrm{RMS}}}$ data fall below the best-fit curve at higher values of Re_τ.

Given the differences in the evolutions of $\langle \tau_w \rangle$ and $\tau_{w_{\mathrm{RMS}}}$ with Re_τ, it is logical to study the evolution of the (nondimensionalized) intensity of the wall shear stress fluctuations ($\tau_{w_{\mathrm{RMS}}}/\langle \tau_w \rangle$). To this end, Fig. 2 shows the dependence of $\tau_{w_{\mathrm{RMS}}}/\langle \tau_w \rangle$ on Re_τ. Figure 2(a) depicts the results of the present experiments, plotted in linear-linear coordinates. Figure 2(b) plots the same data along with data from other researchers—both experimental and numerical—in linear-log coordinates. (Note, however, that analogous data recorded in turbulent boundary layers is not included, and only results from turbulent channel flows are plotted, to ensure the most direct of comparisons, even if it can be argued that zero-pressure-gradient boundary layers and fully developed turbulent channel flow have similar near-wall flows and structure). The data in Fig. 2(a) show that the intensity of the wall shear stress fluctuations increases with friction Reynolds number to a point, after which it asymptotes to a constant value (of approximately 0.44). This is indicative of the turbulence achieving a “fully

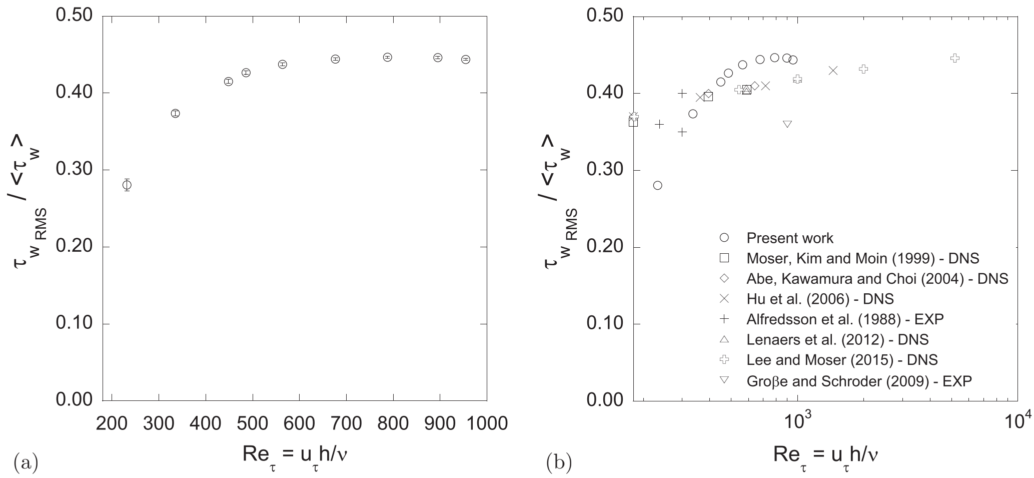

FIG. 2. The dependence of the intensity of the wall shear stress fluctuations on friction Reynolds number (Re_τ). (a) Present work (linear-linear plot). (b) Present work compared with the work of others (linear-log plot). 95% confidence intervals estimated by Bayesian bootstrap analysis [58] using 200 replications are depicted in (a) by way of error bars.

turbulent" state (sometimes, in other contexts [59–61], referred to as "fully developed turbulence," which is a phrasing that is avoided in this work to prevent possible confusion that could arise when discussing fully developed flows in ducts and channels). With respect to the evolution of $\tau_{w_{\mathrm{RMS}}}/\langle\tau_w\rangle$ with Reynolds number, we further note the following. First, it is worth remarking that the plateau in $\tau_{w_{\mathrm{RMS}}}/\langle\tau_w\rangle$ occurs at $\mathrm{Re}_\tau \approx 600$. Second, the asymptotic value of 0.44 is similar to the value found in the ($R_\tau \approx 300$) experiments of Alfredsson *et al.* [30] (0.40). Moreover, our measured asymptotic value of 0.44 is even closer to values obtained by Hu *et al.* [24], Lenaers *et al.* [42], and Lee and Moser [43], who obtained maximum values of 0.43, 0.42, and 0.45, respectively, thus confirming the results of prior high-Reynolds-number direct numerical simulations. (It is also consistent with results from zero-pressure-gradient boundary layers, such as those of Wu and Moin [62], who obtained a value of 0.44). It is not, however, unexpected that the degree of agreement at low Reynolds numbers is not as close as that observed for the asymptotic values of $\tau_{w_{\mathrm{RMS}}}/\langle\tau_w\rangle$ between the present work and those of the high-Reynolds-number DNSs. At lower Reynolds numbers, the differences between various experiments and simulations will be heightened due to the dependence on the various initial and boundary conditions (in both experiments and numerical simulations). At low Reynolds numbers, the flow is not highly turbulent, and it retains a dependence on its initial and boundary conditions, whether they be physical or numerical. The expectation of a universal structure of the wall shear stress field can only be met at high Reynolds numbers, and the values of $\tau_{w_{\mathrm{RMS}}}/\langle\tau_w\rangle$ from various sources do indeed exhibit more similar values as the Reynolds number is increased. Third, even though the present experimental measurements of $\tau_{w_{\mathrm{RMS}}}/\langle\tau_w\rangle$ extend to higher friction Reynolds numbers than any others to date (to the knowledge of the authors), they show no indication of attenuation due to reduced temporal or spatial resolution as the Reynolds number increases. The constancy of $\tau_{w_{\mathrm{RMS}}}/\langle\tau_w\rangle$ at large Re_τ is indicative of the high-frequency response of our wall-shear-stress sensor, which exhibits no sign of attenuation of its response due to a reduced temporal resolution at high frequencies associated with the large Reynolds numbers, as discussed by Alfredsson *et al.* [30]. The high-frequency response of the present sensor is attributed to a design [53,54] in which the thermal time constant is kept as small as possible by eliminating direct contact between the heated element of the sensor and the channel wall (by having a shallow rectangular cavity under it), while maintaining the wire flush with the wall. Furthermore, our sensor gives no indication of reduced spatial resolution as the Reynolds number increases, as observed in prior works (e.g., Colella and Keith [63]) and discussed in detail by Örlü and Schlatter [31]. More precisely, the magnitudes of the asymptotically measured values of $\tau_{w_{\mathrm{RMS}}}/\langle\tau_w\rangle$ show no significant reductions when the wall-unit normalized sensor length ($L^+ \equiv Lu_\tau/\nu$) increases with Re_τ, as has been observed in measurements of wall shear stress by other methods (e.g., flush-mounted hot-films sensors and electrochemical sensors).

Although it stands to reason that the spatial resolution of any wall-shear-stress sensor decreases with increasing Reynolds number, the spanwise dimension of a sensor cannot be the sole factor determining the minimum sensor dimensions, as a sensor's streamwise and temporal resolutions will also play a role in determining the sensor's overall resolution. With respect to the question of the spanwise resolution of wall-shear-stress sensors, Örlü and Schlatter [31] applied a spanwise filter to their DNS data of a turbulent boundary layer and observed an approximately linear decrease in $\tau_{w_{\mathrm{RMS}}}/\langle\tau_w\rangle$ from 0.42 at $L^+ \approx 5$ to 0.31 at $L^+ \approx 60$. However, a clear comparison of their results with the present ones (for which L^+_{wire} lies in the range $9.7 \leqslant L^+_{\mathrm{wire}} \leqslant 39.8$; see Table I) is difficult given the lack of any details on the nature of the averaging process used in Örlü and Schlatter [31] (e.g., in what order and how the filtering and averaging processes were undertaken). Note that the resolution of their DNS in the spanwise direction is $9.6 \leqslant \Delta z^+ \leqslant 10.8$ for $\mathrm{Re}_\theta \equiv U_\infty\theta/\nu = 2500$ to 4300, where U_∞ and θ are the boundary layer's free-stream velocity and momentum thickness, respectively. The streamwise resolution also plays a role in estimates of $\tau_{w_{\mathrm{RMS}}}/\langle\tau_w\rangle$, whether they be experimental or numerical. The streamwise resolution of the DNS of Örlü and Schlatter [31] ($17.9 \leqslant \Delta x^+ \leqslant 25.3$) is coarser than the transverse resolution, but typical of those of state-of-the-art simulations, although some researchers have be able to employ highly refined resolutions (e.g., $\Delta x^+ < 6$ [42,64]). If the sensor areas normalized in wall units [e.g., $A^+ \equiv A/(\nu/u_\tau)^2$] are calculated, then the resolution of the DNS of Ref. [31] is ($A^+ = \Delta x^+ \times \Delta z^+$) 170 to 270, which is larger than the (projected) surface area of the wall-shear-stress sensor used herein ($A^+_{\mathrm{wire}} = D^+_{\mathrm{wire}} L^+_{\mathrm{wire}}$), which is 3.2 at the highest Reynolds number studied. Therefore, it is possible that the effect of the spatial resolution in the spanwise direction may be more prominent if the sensor streamwise dimension is coarser, given that it is clear that the DNS of Örlü and Schlatter [31] is (i) sufficiently resolved when unfiltered and (ii) consistent with all previous and subsequent work in turbulent boundary layers.

Using another approach to investigate the effect of spatial resolution, Lenaers *et al.* [42] performed DNSs of incompressible turbulent channel flow with Reynolds numbers up to $\mathrm{Re}_\tau = 1000$ using three different resolutions ("coarse, medium and fine"). In their simulations, the normalized streamwise (Δx^+), transverse (Δz^+), and area (A^+) resolutions were refined from 18 to 5, 6 to 2.5, and 108 to 12.5, respectively. Moreover, they concluded that the "simulations performed at different resolutions give only minor differences." The qualitative difference in the results of Refs. [31] and [42] may stem from the better transverse (or area) resolution in the latter simulations. Nevertheless, the subject of sensor and numerical resolution on estimates of wall shear stress is clearly one that needs further investigation, as it has received much less attention than analyses of the resolution of the velocity field in turbulent flows. We lastly remark that the temporal resolution of the experiments or simulations may also affect estimates of $\tau_{w_{\mathrm{RMS}}}/\langle\tau_w\rangle$. As alluded to above, it will be shown using the spectra of the wall-shear-stress fluctuations that the present measurements have sufficient temporal resolutions.

To further examine the Reynolds-number-dependence of turbulent channel flow, Fig. 3 depicts the dependence of both the skewness (S_{τ_w}) and kurtosis (K_{τ_w}) of the wall shear stress on the Reynolds number, over the range $230 \leqslant \mathrm{Re}_\tau \leqslant 950$. Similar to the intensity of the wall shear stress fluctuations, the evolutions of both the skewness and kurtosis of τ_w exhibit an increasing trend with Reynolds number, up to $\mathrm{Re}_\tau \approx 600$, at which point the values of S_{τ_w} and K_{τ_w} plateau, maintaining approximately constant values of 1.4 and 6.6, respectively. It is clear that the fluctuations in wall shear stress are notably (and positively) skewed, which is both (i) consistent with previous measurements of wall shear stress (in both channel flows and boundary layers, e.g., [24,30,32,33,38]), and (ii) consistent with the underlying physics of this flow with an unambiguous direction of the

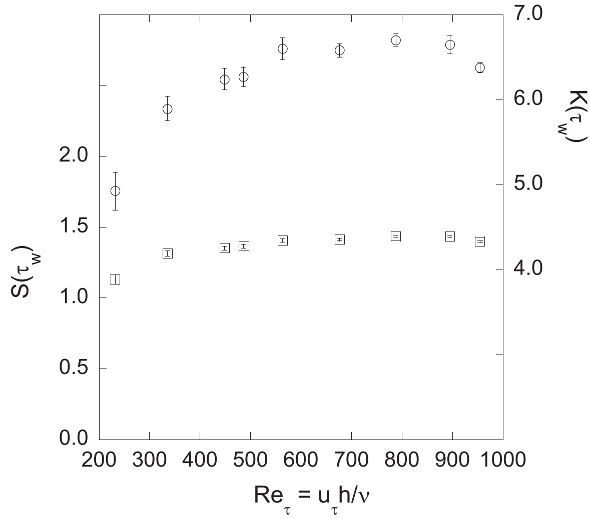

FIG. 3. The dependence of the skewness (□) and kurtosis (○) of the wall shear stress fluctuations on friction Reynolds number (Re_τ). 95% confidence intervals estimated by Bayesian bootstrap analysis [58] using 200 replications are depicted by way of error bars.

mean flow. (Near the wall, positive velocity fluctuations, and therefore positive/forward velocity gradients, will be more likely than negative/backwards ones). In addition to exhibiting positive skewness, the fluctuations in τ_w are also notably super-Gaussian (i.e., $K_{\tau_w} \approx 6.6 > 3$), indicating the large probability of extreme fluctuations in wall shear stress. We also remark that the present measurements of K_{τ_w} are somewhat larger than those observed in previous works, in which K_{τ_w} was found to be approximately 4.8 [30] and up to 5.3 at $Re_\tau = 1440$ [24]. This finding will be discussed in more detail in the context of the PDFs of τ_w.

The nature of the distribution of τ_w is further investigated by studying its probability density function in Fig. 4, which plots the (normalized) PDF of fluctuations in τ_w for four Reynolds

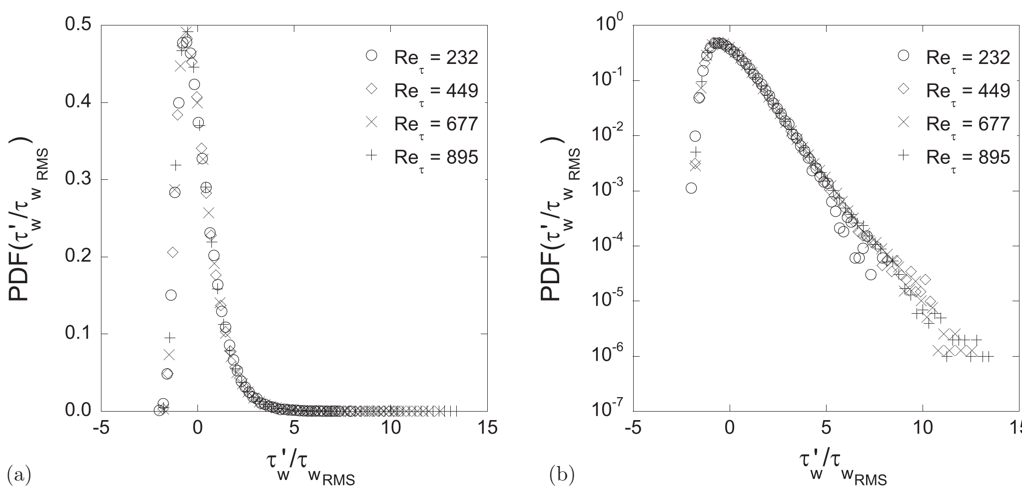

FIG. 4. Normalized probability density functions (PDFs) of the wall shear stress fluctuations for Re_τ = 232, 449, 677, and 895. (a) Linear-linear axes. (b) Log-linear axes. Recall $\tau'_w = \tau_w - \langle\tau_w\rangle$.

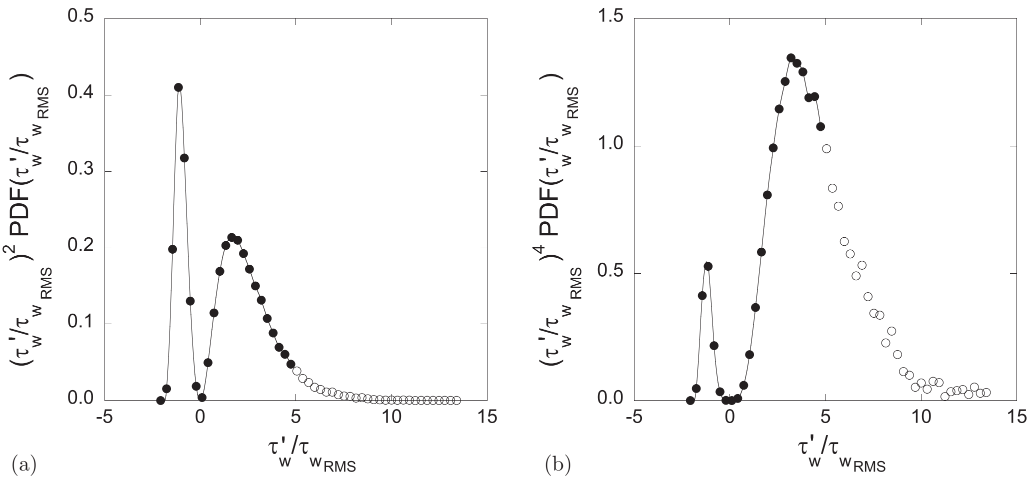

FIG. 5. Normalized PDFs of the wall shear stress fluctuations multiplied by (a) $(\tau_w/\tau_{w_{\mathrm{RMS}}})^2$, and (b) $(\tau_w/\tau_{w_{\mathrm{RMS}}})^4$. The area under these curves are equal to the normalized second and fourth moments of the wall shear stress. The area under the open circles represents the contribution to the moment that would be unresolved if fluctuations greater than 5 standard deviations were not accounted for. $\mathrm{Re}_\tau = 895$.

numbers ($\mathrm{Re}_\tau = 232,\ 449,\ 677$, and 895). As can be observed, the collapse of the PDFs, when plotted nondimensionally, is excellent, which is consistent with data that is both converged and of high signal-to-noise ratio. The only (minor) outliers—that can only be observed when plotting the PDFs in log-linear coordinates [Fig. 4(b)]—are for the lowest Reynolds number ($\mathrm{Re}_\tau = 232$). This difference is presumably related to the fact that the flow at this low Reynolds number has yet to reach its asymptotic state, as also observed in Figs. 2 and 3. As Re_τ increases, it is also of interest to observe how the maximum measured values of the normalized wall shear stress increase. At $\mathrm{Re}_\tau = 232,\ 449,\ 677$ and 895, $\tau_{w'_{\max}}/\tau_{w_{\mathrm{RMS}}}$ is, respectively, 7.9, 10.4, 12.6, and 13.4. Therefore, even though the shape of the normalized PDF of τ_w does not significantly change, the extent of the largest measured values of wall shear stress continually increases.

The present values of K_{τ_w} are larger than those previously measured due to our (i) sensor's ability to measure large, but rare, fluctuations in τ_w, and (ii) lengthy sampling durations, increasing the probability of the large, rare fluctuations being measured. Note that the PDFs of $\tau'_w/\tau_{w_{\mathrm{RMS}}}$ in the works of Obi *et al.* [32], Miyagi *et al.* [33], Khoo *et al.* [34], Keirsbulck *et al.* [38] did not extend beyond values of $\tau'_w/\tau_{w_{\mathrm{RMS}}}$ equal to 4, 6, 5, and 7.5, respectively, and these authors measured kurtoses of the wall shear stress of 4.6–4.7, 4.6, 4.9, and 4.8, respectively. Moreover, if we truncate the present PDF such that it is zero for values of $\tau'_w/\tau_{w_{\mathrm{RMS}}} > 5$ and recalculate the kurtosis, then we obtain a value of 4.71—a value that is consistent with the results of prior researchers. This agreement thus emphasizes the importance in resolving the large, rare fluctuations in τ_w, which can have a notable effect on its statistical moments. With respect to the third- and second-order statistical moments, we find that truncating the PDF of τ_w (so that there are no data above $\tau'_w/\tau_{w_{\mathrm{RMS}}} = 5$) causes the skewness to reduce to 1.13 and the turbulent intensity of τ_w to 0.427, which is also in agreement with the values of these quantities measured by previous researchers. It is thus clear that the need to resolve the large and rare fluctuations in wall shear stress can have a substantial effect on the statistics of τ_w, especially at higher orders, where the tails of the PDF play an increasingly important role in determining their magnitude. This phenomenon is graphically depicted in Figs. 5(a) and 5(b), which plot the PDF of the normalized wall shear stress multiplied by $(\tau'_w/\tau_{w_{\mathrm{RMS}}})^n$ at second ($n = 2$) and fourth ($n = 4$) order, respectively, for $\mathrm{Re}_\tau = 895$. The area under these curves are equal to the normalized second and fourth moments of the wall shear stress. If the PDFs do not extend past $\tau'_w/\tau_{w_{\mathrm{RMS}}} = 5$, then it is clear that the integral under these curves will be unclosed and that (i) the second-order moment of the wall shear stress (which is related to the square of the turbulent intensity) will be slightly underestimated, and (ii) the fourth-order moment (related to the kurtosis) will be substantially underestimated. It is also worth noting that the (unavoidable) scatter in the PDF of $\tau_w'/\tau_{w_{\rm RMS}}$ for large, rare fluctuations ($\tau_w'/\tau_{w_{\rm RMS}} > 10$) does not significantly impact estimated of the kurtosis. Filtering the values of $\tau_w'/\tau_{w_{\rm RMS}} > 10$ from the PDF only reduces the kurtosis by 2%. Moreover, its effect on lower-order statistics will be even smaller.

We also remark that the PDFs of the wall shear stress fluctuations in Fig. 4(b) *seem* to indicate that negative values of the wall shear stress fluctuations, corresponding to flow reversals, are effectively not detected, with the absence of wall shear stress measurements below $\tau_w'/\tau_{w_{\rm RMS}} = -2$. [Because (i) the abscissa in Fig. 4 correspond to the *fluctuations* in wall shear stress, and (ii) $\tau_{w_{\rm RMS}}/\langle\tau_w\rangle \approx 0.44$, the value of zero instantaneous wall shear stress in these plots corresponds to $\tau_w'/\tau_{w_{\rm RMS}} = -(\tau_{w_{\rm RMS}}/\langle\tau_w\rangle)^{-1} \approx -2.3$]. Given the unidirectional nature of the mean flow and the strong [$\mathcal{O}(1)$] subsequent positive skewness of τ_w, this could be expected. However, the dearth of measured fluctuations in wall shear stress may also be related to the inability of our sensor to distinguish between positive and negative values of wall shear stress. This phenomenon is akin to the inability of a hot-wire anemometer to measure negative velocities, and exists for most other thermal or electrochemical wall shear stress sensors (with a notable exception being the sensor of Spazzini *et al.* [53]). Nevertheless, as can be seen in Fig. 4(a), both the positive and negative tails of the PDF of τ_w approach values of zero very closely.

The issue of negative values of the wall-shear stress fluctuations and flow reversals have mostly been studied by those undertaking simulations, with some exceptions, such as the work of Brücker [65], who experimentally observed flow reversals using a micropillar array. The DNS of Örlü and Schlatter [31] indicated that the contribution of negative wall shear stress values in a turbulent boundary layer is less than 0.1% of the PDF. Similarly, Hu *et al.* [24] observed from their DNS of turbulent channel flows that the probability of negative wall shear stress values varied from 0.0030% at $\mathrm{Re}_\tau = 90$ to 0.085% $\mathrm{Re}_\tau = 1440$. Further insight into the question of negative wall shear stress fluctuations was provided by Lenaers *et al.* [42], who investigated the existence of negative streamwise velocities in the near-wall region ($y^+ \leqslant 5$). Lenaers *et al.* [42] observed that the occurrence of near-wall negative velocities increased with increasing Reynolds number, from 0.01% of velocities at $\mathrm{Re}_\tau = 180$ to 0.06% at $\mathrm{Re}_\tau = 1000$. Moreover, Lenaers *et al.* [42] also observed that the region in which negative velocities occurred increased with increasing Reynolds number. They found that the region of negative streamwise velocities extended up to $y^+ \approx 4.5$ at $\mathrm{Re}_\tau = 180$, and up to $y^+ \approx 8.5$ at $\mathrm{Re}_\tau = 1000$. They also noted that the amount of backflows reduced only slightly when they increased the resolution of their simulations.

Given that the above results have demonstrated that negative values of the wall shear stress fluctuations and/or negative streamwise velocity fluctuations do not seem to exceed 0.1% of the total amount, the insensitivity of our sensor to negative values of wall shear stress fluctuations will have a negligible effect on the statistics of τ_w presented herein—especially the lowest order ones, such as the turbulent intensity of the wall shear stress ($\tau_{w_{\rm RMS}}/\langle\tau_w\rangle$). This is further confirmed by noting that the area under the compensated PDF in Figs. 4(a) and 4(b) would not change were the PDF extended to values $\tau_w'/\tau_{w_{\rm RMS}} < -2.3$, as the PDF is effectively zero at that point.

Lastly, the power spectral densities (referred to from hereon in as "spectra") of the wall shear stress fluctuations are plotted for the same four Reynolds numbers as the PDFs in Fig. 6(a). As the Reynolds number increases, the magnitude of the fluctuations of τ_w both increase and extend to higher frequencies. The low-frequency plateaux of the spectra increase by roughly two orders of magnitude—an observation that is consistent with the results of Fig. 1(b), which exhibited an increase in $\tau_{w_{\rm RMS}}$ of approximately one order of magnitude. (Recall that the integral under the spectra is equal to the variance, which is the square of the RMS value.) Note the high signal-to-noise ratio that can be achieved with the present sensor, which extends over nearly 6 decades (10^{-10} to 10^{-4}) for the $\mathrm{Re}_\tau = 895$ spectrum. Such a result is generally achievable only with hot-wire anemometry, and requires significant computing power to reach similar levels in numerical simulations (e.g., Hu *et al.* [24]).

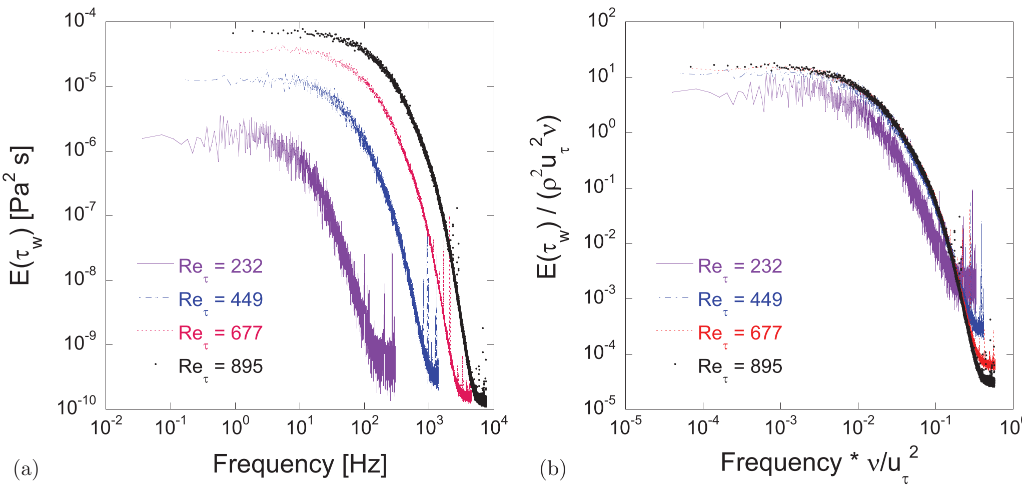

FIG. 6. Power spectral densities of the wall shear stress fluctuations for $\mathrm{Re}_\tau = 232$, 449, 677, and 895. (a) Dimensional spectra. (b) Spectra nondimensionalized using wall units.

In Fig. 6(b), we plot the spectra of Fig. 6(a) nondimensionalized using wall units. Note that at the highest Reynolds numbers, the collapse of the spectra is excellent, further supporting the notion of an asymptotic regime being achieved once the Reynolds number is sufficiently large, consistent with the previous results in Figs. 2, 3, and 4.

In the absence (to the authors' knowledge) of any theoretical predictions for the shape of the spectra of wall shear stress fluctuations, we further remark that the spectra of τ_w do not exhibit distinct power-law subranges at any of the Reynolds numbers studied herein. Given that the wall shear stress is intrinsically dependent on the viscosity of the fluid, the absence of an "inertial" subrange (i.e., a range of scales independent of the fluid's viscosity) could be expected. Nevertheless, measurements at even higher Reynolds numbers beyond those studied herein could lend further insight. However, it is also worth commenting on the similarity in the shape of the wall-shear-stress spectra with spectra of (transverse) derivatives of a turbulent quantity (ϕ). It can be shown (e.g., Van Atta [66]) that although the power spectrum of the longitudinal derivative of velocity or a passive scalar ($\partial\phi/\partial x$) exhibits a inertial range power law (generally increasing as $k^{1/3}$, where k is the longitudinal wave number) which peaks at small scales, but then decreases toward zero as the Kolmogorov microscale is approached, the power spectra of $\partial\phi/\partial y$ and $\partial\phi/\partial z$ at a given wave number are monotonically decreasing functions of wave number with no local maxima, if isotropy is assumed. The explanation for this different behavior is that the spectra of transverse derivatives can be expressed as integrals of the spectra of their respective longitudinal derivatives, from that same wave number to infinity (Van Atta [66, p. 142]). The present power spectra of the wall shear stress are observed to be monotonically decreasing functions of frequency (to within the experimental uncertainty in the estimation of the power spectra), consistent with the behavior of power spectra of longitudinal derivatives discussed by Van Atta [66]. Given the realization that the spectrum of the (longitudinal component) of the wall shear stress is the equivalent to the spectrum of $\partial u/\partial y$ (evaluated at $y = 0$), such a form is indeed consistent with the arguments of Van Atta [66].

IV. CONCLUSIONS

Using the wall-shear-stress sensor of Afara *et al.* [55], which was inspired by that of Spazzini *et al.* [53] and Sturzebecher *et al.* [54], we have methodologically studied the evolution of the wall shear stress with Reynolds numbers by way of measurements in fully developed turbulent flows in a high-aspect-ratio channel, over the range $230 \leqslant \mathrm{Re}_\tau \leqslant 950$. High-resolution measurements of the wall shear stress, with strong signal-to-noise ratio, were obtained and depicted a tendency toward an asymptotic state, when suitably nondimensionalized. The turbulent intensity of the wall shear stress, $\tau_{w_{\mathrm{RMS}}}/\langle\tau_w\rangle$, increases monotonically with Reynolds number, and asymptotes to a value of approximately 0.44 for $\mathrm{Re}_\tau \gtrsim 600$. Similarly, the skewness and kurtosis of τ_w increase with Reynolds number and were found to asymptote to values of 1.4 and 6.6, respectively, for Reynolds numbers above $\mathrm{Re}_\tau \sim 600$. When suitably nondimensionalized, the PDFs of τ_w exhibited excellent collapse for the different Reynolds numbers and showed very large fluctuations in τ_w (beyond 10 standard deviations in τ_w for the highest Reynolds numbers), above what is generally detected when measuring the PDF of the velocity field in similar flows. Furthermore, the ability to measure the large but rare fluctuations in τ_w were shown to be crucial to obtaining accurate estimates of the statistical moments of τ_w, and the effect of insufficiently resolving the full range of fluctuations in the wall shear stress on its statistical moments was demonstrated. As the Reynolds number was increased, the power spectra of τ_w exhibited an increasing range of (i) frequencies over which wall shear stress fluctuations occurred, and (ii) intensity of the wall shear stress fluctuations. The spectra of τ_w were also found to collapse using a wall-unit-based normalization once the Reynolds number was sufficiently large, further validating the existence of an asymptotic high-Reynolds-number state of τ_w beyond $\mathrm{Re}_\tau \sim 600$.

ACKNOWLEDGMENTS

This work was graciously funded by the Natural Sciences and Engineering Research Council (NSERC) of Canada (Grants No. RGPIN 217184-2013 (L.M.) and No. RGPIN 03674-2014 (B.R.B.), respectively). J.M. was supported by a NSERC Canada Graduate Scholarship. J.S. was supported by way of a NSERC Undergraduate Student Research Award.

[1] A. Kolmogorov, The local structure of turbulence in incompressible viscous fluid for very large Reynolds numbers, Dokl. Akad. Nauk. SSSR **30**, 301 (1941).

[2] K. R. Sreenivasan and R. A. Antonia, The phenomenology of small-scale turbulence, Annu. Rev. Fluid Mech. **29**, 435 (1997).

[3] R. A. Antonia, B. R. Satyaprakash, and A. J. Chambers, Reynolds number dependence of velocity structure functions in turbulent shear flows, Phys. Fluids **25**, 29 (1982).

[4] R. A. Antonia, S. Rajagopalan, C. S. Subramanian, and A. J. Chambers, Reynolds-number dependence of the structure of a turbulent boundary layer, J. Fluid Mech. **121**, 123 (1982).

[5] L. Mydlarski and Z. Warhaft, On the onset of high-Reynolds-number grid-generated wind tunnel turbulence, J. Fluid Mech. **320**, 331 (1996).

[6] J. Qian, Inertial range and the finite Reynolds number effect of turbulence, Phys. Rev. E **55**, 337 (1997).

[7] S. Mochizuki and F. T. M. Nieuwstadt, Reynolds-number-dependence of the maximum in the streamwise velocity fluctuations in wall turbulence, Exp. Fluids **21**, 218 (1996).

[8] M. V. Zagarola and A. J. Smits, Mean-flow scaling of turbulent pipe flow, J. Fluid Mech. **373**, 33 (1998).

[9] L. Danaila, F. Anselmet, T. Zhou, and R. A. Antonia, A generalization of Yaglom's equation which accounts for the large-scale forcing in heated decaying turbulence, J. Fluid Mech. **391**, 359 (1999).

[10] R. A. Antonia, B. R. Pearson, and T. Zhou, Reynolds number dependence of second-order velocity structure functions, Phys. Fluids **12**, 3000 (2000).

[11] G. P. Romano and R. A. Antonia, Longitudinal and transverse structure functions in a turbulent round jet: Effect of initial conditions and Reynolds number, J. Fluid Mech. **436**, 231 (2001).

[12] G. Boffetta and G. P. Romano, Structure functions and energy dissipation dependence on Reynolds number, Phys. Fluids **14**, 3453 (2002).

[13] J. Lepore and L. Mydlarski, Effect of the Scalar Injection Mechanism on Passive Scalar Structure Functions in a Turbulent Flow, Phys. Rev. Lett. **103**, 034501 (2009).

[14] J. C. Klewicki, Reynolds number dependence, scaling, and dynamics of turbulent boundary layers, J. Fluids Eng. **132**, 094001 (2010).

[15] A. J. Smits, B. J. McKeon, and I. Marusic, High-Reynolds number wall turbulence, Ann. Rev. Fluid Mech. **43**, 353 (2011).

[16] M. Hultmark, M. Vallikivi, S. C. C. Bailey, and A. J. Smits, Turbulent Pipe Flow at Extreme Reynolds Numbers, Phys. Rev. Lett. **108**, 094501 (2012).

[17] J. Tchoufag, P. Sagaut, and C. Cambon, Spectral approach to finite Reynolds number effects on Kolmogorov's 4/5 law in isotropic turbulence, Phys. Fluids **24**, 015107 (2012).

[18] J. Lepore and L. Mydlarski, Finite-Péclet-number effects on the scaling exponents of high-order passive scalar structure functions, J. Fluid Mech. **713**, 453 (2012).

[19] S. L. Tang, R. A. Antonia, L. Djenidi, L. Danaila, and Y. Zhou, Finite Reynolds number effect on the scaling range behavior of turbulent longitudinal velocity structure functions, J. Fluid Mech. **820**, 341 (2017).

[20] R. A. Antonia, L. Djenidi, L. Danaila, and S. L. Tang, Small-scale turbulence and the finite Reynolds number effect, Phys. Fluids **29**, 020715 (2017).

[21] L. Mydlarski and Z. Warhaft, Passive scalar statistics in high-Péclet-number grid turbulence, J. Fluid Mech. **358**, 135 (1998).

[22] M. Fischer, J. Jovanovic, and F. Durst, Reynolds number effects in the near-wall region of turbulent channel flows, Phys. Fluids **13**, 1755 (2001).

[23] H. Abe, H. Kawamura, and H. Choi, Very large-scale structures and their effects on the wall shear-stress fluctuations in a turbulent channel flow up to $\mathrm{Re}_\tau = 640$, J. Fluids Eng., Trans. ASME **126**, 835 (2004).

[24] Z. W. Hu, C. L. Morfey, and N. D. Sandham, Wall pressure and shear stress spectra from direct simulations of channel flow, AIAA J. **44**, 1541 (2006).

[25] J. E. Mitchell and T. J. Hanratty, A study of turbulence at a wall using an electrochemical wall shear-stress meter, J. Fluid Mech. **26**, 199 (1966).

[26] A. T. Popovich, Statistical analysis of fluid flow fluctuations in the viscous layer near a solid wall, Ind. Eng. Chem. Fund. **8**, 609 (1969).

[27] H. Eckelmann, The structure of the viscous sublayer and the adjacent wall region in a turbulent channel flow, J. Fluid Mech. **65**, 439 (1974).

[28] K. R. Sreenivasan and R. A. Antonia, Properties of wall shear stress fluctuations in a turbulent duct flow, J. Appl. Mech. Trans ASME **44**, 389 (1977).

[29] F. W. Chambers, H. D. Murphy, and D. M. McEligot, Laterally converging flow. Part 2. Temporal wall shear stress, J. Fluid Mech. **127**, 403 (1983).

[30] P. H. Alfredsson, A. V. Johansson, J. H. Haritonidis, and H. Eckelmann, The fluctuating wall-shear stress and the velocity field in the viscous sublayer, Phys. Fluids **31**, 1026 (1988).

[31] R. Örlü and P. Schlatter, On the fluctuating wall-shear stress in zero pressure-gradient turbulent boundary layer flows, Phys. Fluids **23**, 021704 (2011).

[32] S. Obi, K. Inoue, T. Furukawa, and S. Masuda, Experimental study on the statistics of wall shear stress in turbulent channel flows, Int. J. Heat Fluid Flow **17**, 187 (1996).

[33] N. Miyagi, M. Kimura, H. Shoji, A. Saima, C.-M. Ho, S. Tung, and Y.-C. Tai, Statistical analysis on wall shear stress of turbulent boundary layer in a channel flow using micro-shear stress imager, Int. J. Heat Fluid Flow **21**, 576 (2000).

[34] B. C. Khoo, Y. T. Chew, and C. J. Teo, Near-wall hot-wire measurements. Part II: Turbulence timescale, convective velocity and spectra in the viscous sublayer, Exp. Fluids **31**, 494 (2001).

[35] S. Große and W. Schröder, Dynamic wall-shear stress measurements in turbulent pipe flow using the micropillar sensor MPS3, Int. J. Heat Fluid Flow **29**, 830 (2008).

[36] S. Große and W. Schröder, Two-dimensional visualization of turbulent wall shear stress using micropillars, AIAA J. **47**, 314 (2009).

[37] E. P. Gnanamanickam, B. Nottebrock, S. Große, J. P. Sullivan, and W. Schröder, Measurement of turbulent wall shear-stress using micro-pillars, Meas. Sci. Tech. **24**, 124002 (2013).

[38] L. Keirsbulck, L. Labraga, and M. Gad-El-Hak, Statistical properties of wall shear stress fluctuations in turbulent channel flows, Int. J. Heat Fluid Flow **37**, 1 (2012).
[39] O. Amili, M. D. Hind, J. W. Naughton, and J. Soria, Evaluation of a film-based wall shear stress measurement technique in a turbulent channel flow, Exp. Thermal Fluid Sci. **70**, 437 (2016).
[40] J. Kim, P. Moin, and R. Moser, Turbulence statistics in fully developed channel flow at low Reynolds number, J. Fluid Mech. **177**, 133 (1987).
[41] R. D. Moser, J. Kim, and N. N. Mansour, Direct numerical simulation of turbulent channel flow up to $\mathrm{Re}_\tau = 590$, Phys. Fluids **11**, 943 (1999).
[42] P. Lenaers, Q. Li, G. Brethouwer, P. Schlatter, and R. Örlü, Rare backflow and extreme wall-normal velocity fluctuations in near-wall turbulence, Phys. Fluids **24**, 035110 (2012).
[43] M. Lee and R. D. Moser, Direct numerical simulation of turbulent channel flow up to $Re_\tau \approx 5200$, J. Fluid Mech. **774**, 395 (2015).
[44] R. Vinuesa, E. Bartrons, Daniel D. Chiu, K. M. Dressler, J.-D. Rüedi, Y. Suzuki, and H. M. Nagib, New insight into flow development and two dimensionality of turbulent channel flows, Exp. Fluids **55**, 1759 (2014).
[45] R. Vinuesa, P. Schlatter, and H. M. Nagib, On minimum aspect ratio for duct flow facilities and the role of sidewalls in generating secondary flows, J. Turbul. **16**, 588 (2015).
[46] R. Vinuesa, P. Schlatter, and H. M. Nagib, Secondary flow in turbulent ducts with increasing aspect ratio, Phys. Rev. Fluids **3**, 054606 (2018).
[47] J. Lepore and L. Mydlarski, Lateral dispersion from a concentrated line source in turbulent channel flow, J. Fluid Mech. **678**, 417 (2011).
[48] R. A. Lavertu and L. Mydlarski, Scalar mixing from a concentrated source in turbulent channel flow, J. Fluid Mech. **528**, 135 (2005).
[49] E. Costa-Patry and L. Mydlarski, Mixing of two thermal fields emitted from line sources in turbulent channel flow, J. Fluid Mech. **609**, 349 (2008).
[50] E. Germaine, L. Mydlarski, and L. Cortelezzi, Evolution of the scalar dissipation rate downstream of a concentrated line source in turbulent channel flow, J. Fluid Mech. **749**, 227 (2014).
[51] S. Beaulac and L. Mydlarski, Dependence on the initial conditions of scalar mixing in the turbulent wake of a circular cylinder, Phys. Fluids **16**, 3161 (2004).
[52] A. Berajeklian and L. Mydlarski, Simultaneous velocity-temperature measurements in the heated wake of a cylinder with implications for the modeling of turbulent passive scalars, Phys. Fluids **23**, 055107 (2011).
[53] P. G. Spazzini, G. Iuso, M. Onorato, and N. Zurlo, Design, test and validation of a probe for time-resolved measurement of skin friction, Meas. Sci. Tech. **10**, 631 (1999).
[54] D. Sturzebecher, S. Anders, and W. Nitsche, The surface hot wire as a means of measuring mean and fluctuating wall shear stress, Exp. Fluids **31**, 294 (2001).
[55] S. Afara, J. Medvescek, L. Mydlarski, B. R. Baliga, and M. MacDonald, Development of a wall-shear-stress sensor and measurements in mini-channels with partial blockages, Exp. Fluids **55**, 1734 (2014).
[56] AMSE-PTC-19.1-2005, Test Uncertainty - AMSE Performace Test Code, 2005.
[57] S. Rezaeiravesh, R. Vinuesa, M. Liefvendahl, and P. Schlatter, Assessment of uncertainties in hot-wire anemometry and oil-film interferometry measurements for wall-bounded turbulent flows, Eur. J. Mech. B/Fluids **72**, 57 (2018).
[58] B. Efron and R. J. Tibshirani, *An Introduction to the Bootstrap* (Chapman & Hall/CRC, Boca Raton, FL, 1993).
[59] R. Benzi, G. Paladin, G. Parisi, and A. Vulpiani, On the multifractal nature of fully developed turbulence and chaotic systems, J. Phys. A **17**, 3521 (1984).
[60] M. Nelkin, Universality and scaling in fully developed turbulence, Adv. Phys. **43**, 143 (1994).
[61] G. I. Barenblatt and N. Goldenfeld, Does fully developed turbulence exist? Reynolds number independence versus asymptotic covariance, Phys. Fluids **7**, 3078 (1995).
[62] X. Wu and P. Moin, Transitional and turbulent boundary layer with heat transfer, Phys. Fluids **22**, 085105 (2010).
[63] K. J. Colella and W. L. Keith, Measurements and scaling of wall shear stress fluctuations, Exp. Fluids **34**, 253 (2003).

[64] X. Wu and P. Moin, Direct numerical simulation of turbulence in a nominally zero-pressure-gradient flat-plate boundary layer, J. Fluid Mech. **630**, 5 (2009).
[65] Ch. Brücker, Evidence of rare backflow and skin-friction critical points in near-wall turbulence using micropillar imaging, Phys. Fluids **27**, 031705 (2015).
[66] C. Van Atta, Local isotropy of the smallest scales of turbulent scalar and velocity fields, Proc. Roy. Soc. A Math. Phys. Eng. Sci. **434**, 139 (1991).